Article

Heterometallic Titanium—Organic Frameworks by Metal-Induced Dynamic Topological Transformations

Natalia M. Padial,* Belén Lerma-Berlanga, Neyvis Almora-Barrios, Javier Castells-Gil, Iván da Silva, María de la Mata, Sergio I. Molina, Jesús Hernández-Saz, Ana E. Platero-Prats, Sergio Tatay, and Carlos Martí-Gastaldo*

Read Online

ACCESS | 📊 Metrics & More | 📰 Article Recommendations | 🆂🅸 Supporting Information

ABSTRACT: Reticular chemistry has boosted the design of thousands of metal and covalent organic frameworks for unlimited chemical compositions, structures, and sizable porosities. The ability to generate porous materials at will on the basis of geometrical design concepts is responsible for the rapid growth of the field and the increasing number of applications derived. Despite their promising features, the synthesis of targeted homo- and heterometallic titanium—organic frameworks amenable to these principles is relentlessly limited by the high reactivity of this metal in solution that impedes the controlled assembly of titanium molecular clusters. We describe an unprecedented methodology for the synthesis of heterometallic titanium frameworks by metal-exchange reactions of MOF crystals at temperatures below those conventionally used in solvothermal synthesis. The combination of hard (titanium) and soft (calcium) metals in the heterometallic nodes of MUV-10(Ca) enables controlled metal exchange in soft positions for the generation of heterometallic secondary building units (SBUs) with variable nuclearity, controlled by the metal incorporated. The structural information encoded in the newly formed SBUs drives an MOF-to-MOF conversion into bipartite nets compatible with the connectivity of the organic linker originally present in the crystal. Our simulations show that this transformation has a thermodynamic origin and is controlled by the terminations of the (111) surfaces of the crystal. The reaction of MUV-10(Ca) with first-row transition metals permits the production of crystals of MUV-101(Fe,Co,Ni,Zn) and MUV-102(Cu), heterometallic titanium MOFs isostructural with archetypical solids such as MIL-100 and HKUST. In comparison to de novo synthesis, this metal-induced topological transformation provides control over the formation of hierarchical micro-/mesopore structures at different reaction times and enables the formation of heterometallic titanium MOFs not accessible under solvothermal conditions at high temperature, thus opening the door for the isolation of additional titanium heterometallic phases not linked exclusively to trimesate linkers.

MUV-101(Fe,Co,Ni,Zn)   MUV-10(Ca)   MUV-102(Cu)
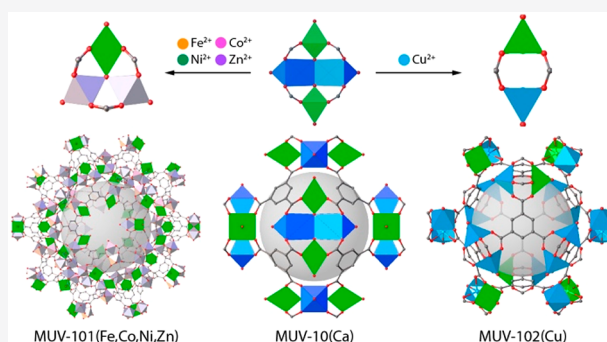
INTRODUCTION

Metal−organic frameworks (MOFs) are crystalline extended structures assembled by the linkage of inorganic polynuclear clusters, termed secondary building units (SBUs), and organic linkers. For the last 15 years, the principles of reticular chemistry have guided the design of thousands of MOFs by rationalizing the combination of SBUs and organic linkers with variable extension points into predetermined topologies.[1] Reticular chemistry provides control over the design of materials at a molecular level for a rich landscape of chemical compositions, structures, and sizable porosities for direct application in gas storage,[2,3] separation,[4−6] or catalysis.[7,8] The rapid growth of the MOF field has built upon two main design strategies. The first, the isoreticular approach, is based on the reticulation of sizable organic linkers of the same geometry and connectivity. It makes it possible to control the metrics and functionality of a specific framework topology that is fixed by

the structural information encoded in the inorganic SBU.[9] The second, the SBU approach, is more general in conception, as it permits targeting multiple MOF topologies also amenable to isoreticular functionalization, by controlling the geometry and connection points of the two building units in the framework.[10,11] The successful translation of these geometric design principles to the synthesis of binary MOFs relies on finding the experimental conditions that reproduce the structural information encoded in the two chemical building units targeted. This is not a problem for the organic linker, which

will retain its geometry and connectivity in solution, but predicting the formation of persistent metal−oxo clusters under crystal growth formation conditions is not straightforward. The chemistry of SBUs intrinsic to archetypical families of MOFs such as $[Cu_2(H_2O)_2(RCO_2)_2]$ (HKUST),[12] $[Cr_3O-(H_2O)_3(RCO_2)_6]$ (MIL-100, MIL-101),[13,14] $[Zn_4O(RCO_2)_6]$ (MOF-5),[9] and $[Zr_6O_4(OH)_4(RCO_2)_{12}]$ (UiO)[15] is well understood and central to the thousands of works related to these materials published in the last years.

With the advance of the field, the application of MOFs has stressed their limitations, calling for enhanced thermal, mechanical, or hydrolytical stabilities and increasing levels of complexity.[16,17] The chemistry of the SBU can be used to improve the thermodynamic stability and tune the chemical reactivity of MOFs. For instance, inorganic clusters based on tetravalent metals such as Ti(IV), Zr(IV), and Hf(IV) are less prone to hydrolysis due to strong M−O bonds. Among these metals, titanium is less toxic, more abundant, and redox active. Still, the synthesis of predesigned titanium frameworks from targeted SBUs remains very challenging due to the high reactivity of Ti salts, which generally lead to ill-defined amorphous phases under solvothermal conditions. On the other hand, complexity at the SBU can be achieved by the combination of two or more metals in heterometallic clusters for mixed-metal MOFs that can outperform their mono-metallic counterparts in different applications such as gas storage, separation, and heterogeneous catalysis.[18,19] The intrinsic properties of Ti-MOFs make this possibility even more appealing, as high stability might be combined with a tailorable electronic structure, photoactivity, or chemical reactivity. However, the limitations of the chemistry of titanium are even more restrictive in this case and there is no straightforward route for their synthesis. The success of one-step synthesis relies on the use of metal ions with similar charges and ionic radii. The high polarizing power of Ti^{4+} prevents a direct reaction with other metals that would likely result in poor control over their distribution in the final material for the formation of segregated phases. In turn, incorporation of other metals into Ti-MOFs by postsynthetic exchange would be inadequate due to the high stability of Ti−O coordination bonds, whereas the incorporation of Ti^{4+} in preformed materials would not allow for complete metal replacement and lacks control over the positioning of titanium atoms in the structure,[20] which can result in a spurious deposition of metal oxide coatings.[21]

We report an unprecedented methodology for the synthesis of heterometallic titanium frameworks amenable to the principles of reticular chemistry. Instead of relying on the serendipitous discovery of mixed-metal clusters by trial and error, we use MOF crystals to direct the formation of SBUs with variable connection points by transmetalation reactions at 65 °C. The combination of hard and soft metals in the heterometallic nodes of MUV-10 (MUV, Materials of Universidad de Valencia) enables controlled metal exchange in soft positions while the structural integrity is retained. The offset in the coordination geometry upon metal replacement generates a thermodynamically metastable state that evolves into the formation of SBUs of decreased nuclearity and dependent on the metal incorporated. The structural information encoded in the newly formed SBUs drives the formation of bipartite nets compatible with the connectivity of the organic linker originally present in the crystal. This metal-induced topological transformation is a dynamic phenomenon

and can be controlled with time until complete transformation of the material.

RESULTS AND DISCUSSION

Metal-Exchange Reactions in Heterometallic SBUs Combining Labile and Robust Coordination Sites. As commented above, the *de novo* synthesis of heterometallic MOFs is restricted to metals with similar reactivity in solution that allow for a concomitant reaction and avoid the formation of homometallic frameworks. Postsynthetic metal exchange is a more versatile route that enables the incorporation of a broader range of metals for heterometallic compositions not accessible by direct synthesis. Metal exchange reactions typically involve soaking of the MOF in concentrated solutions of the metal to be incorporated. The degree of exchange (often incomplete) is kinetically and thermodynamically controlled by the stability constants of the substituting cations and the strength of the M−O bond in the cluster. This is why precedents of MOF transmetalation are mostly focused on labile SBUs more prone to hydrolysis and metal replacement.[22,23] In contrast, robust MOFs with SBUs featuring strong M^{IV}−O bonds, such as $[Zr_6O_4(OH)_4(RCO_2)_{12}]$, are less likely to undergo metal exchange at the cluster and can suffer from uncontrolled grafting at defective positions[20] or induce the undesired formation of an oxide coating.[21] Thus far, transmetalation reactions have been exclusively focused in homometallic MOFs for either labile or robust SBUs that compromise the stability of the resulting material or limit the metal exchange rate, respectively.

We hypothesized that these limitations might be circumvented by using heterometallic SBUs. The combination of soft (M^{+2}) and hard (M^{+4}) metals at different coordination sites in the cluster might translate into quantitative metal replacement without altering the structure or jeopardizing the chemical stability of the framework.

We decided to explore this concept for the heterometallic titanium framework MUV-10(Ca).[24] This microporous solid can be synthesized in high yields from the direct reaction of a calcium salt with different titanium sources. It displays a three-dimensional *the* topology built from the linking of eight-connected $[Ti_2Ca_2(O)_2(H_2O)_4(RCO_2)_8]$ heterometallic SBUs with btc linkers (btc = benzene-1,3,5-tricarboxylate anion). In comparison to the labile and robust coordination sites in Zn_4 and Zr_6 clusters, Ti_2Ca_2 combines hard Ti^{4+} ions in octahedral sites and capped-trigonal-prismatic soft Ca^{2+} centers more prone to metal exchange (Figure 1). Our recent work
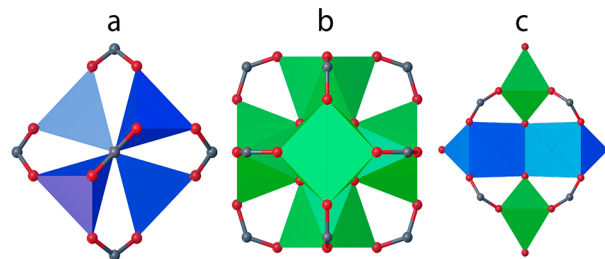

Figure 1. Secondary building units used in transmetalation reactions. Structures of the metal−oxo clusters: (a) $[Zn_4O(RCO_2)_6]$, Zn_4; (b) $[Zr_6O_4(OH)_4(RCO_2)_{12}]$, Zr_6; (c) $[Ti_2Ca_2(O)_2(H_2O)_4(RCO_2)_8]$, Ti_2Ca_2 (this work). Blue and green metal sites denote labile (Zn^{2+}, Ca^{2+}) and robust (Zr^{4+}, Ti^{4+}) metal exchange positions, respectively, red denotes O, and gray denotes C.
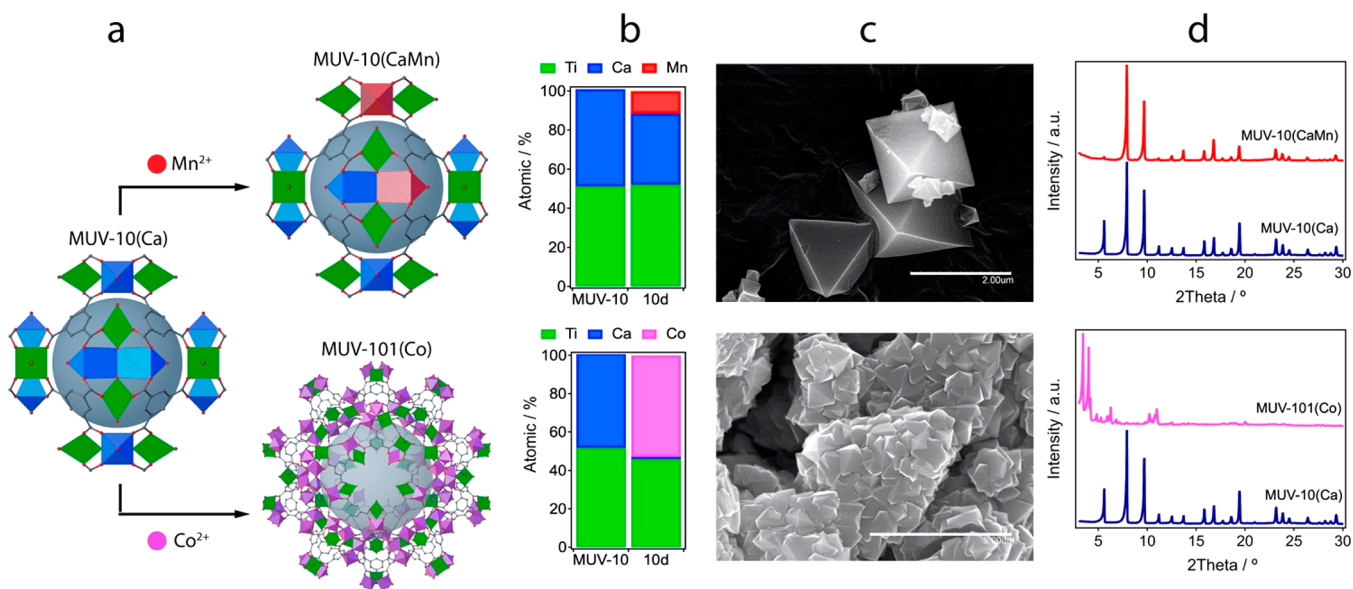
Figure 2. Metal exchange reactions with MUV-10(Ca) crystals: (a) reaction of MUV-10(Ca) in methanolic solutions of Mn^{2+} yields partial metal exchange with retention of the original structure, whereas the same reaction with Co^{2+} drives a topological transformation into MUV-101(Co); (b) experimental metal replacement after 10 days, ;(c) SEM images of the crystals; (d) PXRD after the experiment.

demonstrated the difficulties in producing other heterometallic solids by direct synthesis with divalent first-row transition-metal cations. In contrast to Fe(II), Co(II), Ni(II), Cu(II), and Zn(II), only MUV-10(Mn) could be prepared due to the preference of Mn ions toward a heptacoordinated capped-trigonal-prismatic (CTP) geometry.[24,25] We decided to investigate if same solid could be prepared by transmetalation of the calcium phase. Crystals of MUV-10(Ca) were immersed in concentrated solutions of $Mn(NO_3)_2$ in MeOH (0.2 M) at 65 °C. The resulting MUV-10(CaMn) crystals were filtered and cleaned after 10 days and 30 days for further analyses. We evaluated the degree of metal exchange with X-ray energy dispersive spectroscopy (EDX; section S3.1 in the Supporting Information). The incorporation of Mn is concomitant with a decrease in Ca. Metal exchange is slightly more favorable at longer soaking times; Ca replacement increases from 11.6% (10 days) up to 13.0% after 30 days (Figure 2b, top). In comparison to the postsynthetic modification of Zn_4 clusters in MOF-5,[26] total exchange is far from complete, suggesting thermodynamic control over the transmetalation reaction. The metal distribution was also analyzed with EDX. Mapping throughout the crystals reveals a homogeneous distribution of both metals, ruling out metal clustering at the surface or the formation of segregated phases (section S3.2 in the Supporting Information). Scanning electron microscopy (SEM) confirms that the crystals retained the morphology and micrometer size of the starting material after metal exchange, suggesting a crystal-to-crystal reaction rather than recrystallization in the presence of the new metal (Figure 2c, top). Retention of the original structure was confirmed by powder X-ray diffraction (PXRD) Le Bail refinement of the samples at variable soaking times (Figure 2d (top) and section S3.3 in the Supporting Information). The absence of additional peaks discards the formation of an additional phase upon metal exchange. The changes in the relative intensities of the [100] reflection possibly originates from a preferential orientation of the crystals, as we avoided grinding to prevent amorphization. Crystals were activated by using the protocol reported for

MUV-10(Ca) to analyze the effect of metal exchange over the porosity of the solid (section S3.4 in the Supporting Information). The N_2 isotherm collected confirmed that MUV-10(CaMn) retained the original porosity with an insignificant effect on the BET surface area and the experimental pore diameter. Also important, PXRD data of the crystals after soaking in concentrated HCl and NaOH(aq) solutions confirm that transmetalation does not compromise the hydrolytic stability of the parent solid that originates from the presence of robust Ti−O nodes (section S3.5 in the Supporting Information).

In order to demonstrate if the cluster in MUV-10 might be compatible with the incorporation of other transition-metal ions to access chemical compositions not accessible by direct synthesis, we next attempted the same experiments in the presence of Co^{2+}. Soaking of MUV-10(Ca) in methanolic solutions of $Co(NO_3)_2 \cdot 6H_2O$ (0.2 M) at 65 °C resulted in the formation of a pink solid already after 10 days. In comparison to partial replacement for the Mn case, the EDX analysis revealed that after this time metal exchange became quantitative for the case of Co with only slight traces of unexchanged calcium, close to 0.1% (Figure 2b, bottom). Quantitative metathesis has been reported for labile $[Cd_4O]^{6+}$ units[22] in MOF single crystals, but this drastic increase in substitution on moving from Mn^{2+} to Co^{2+} was unanticipated. To investigate its origin, we inspected the crystals with SEM after the reaction. In comparison to transmetalation with Mn, which does not influence the original morphology, reaction with cobalt induces the formation of a cluster of micrometer-sized crystals with an octahedral morphology that completely occupy the original space of the seeding MUV-10(Ca) crystal (Figure 2c, bottom). EDX mapping of the crystals is again consistent with the formation of a single phase with a homogeneous distribution of Ti and Co throughout the newly formed crystals and complete depletion of Ca. However, PXRD reveals the complete transformation of the original material into a new phase that displays high crystallinity (Figure 2d, bottom). Rather than metal exchange, in the
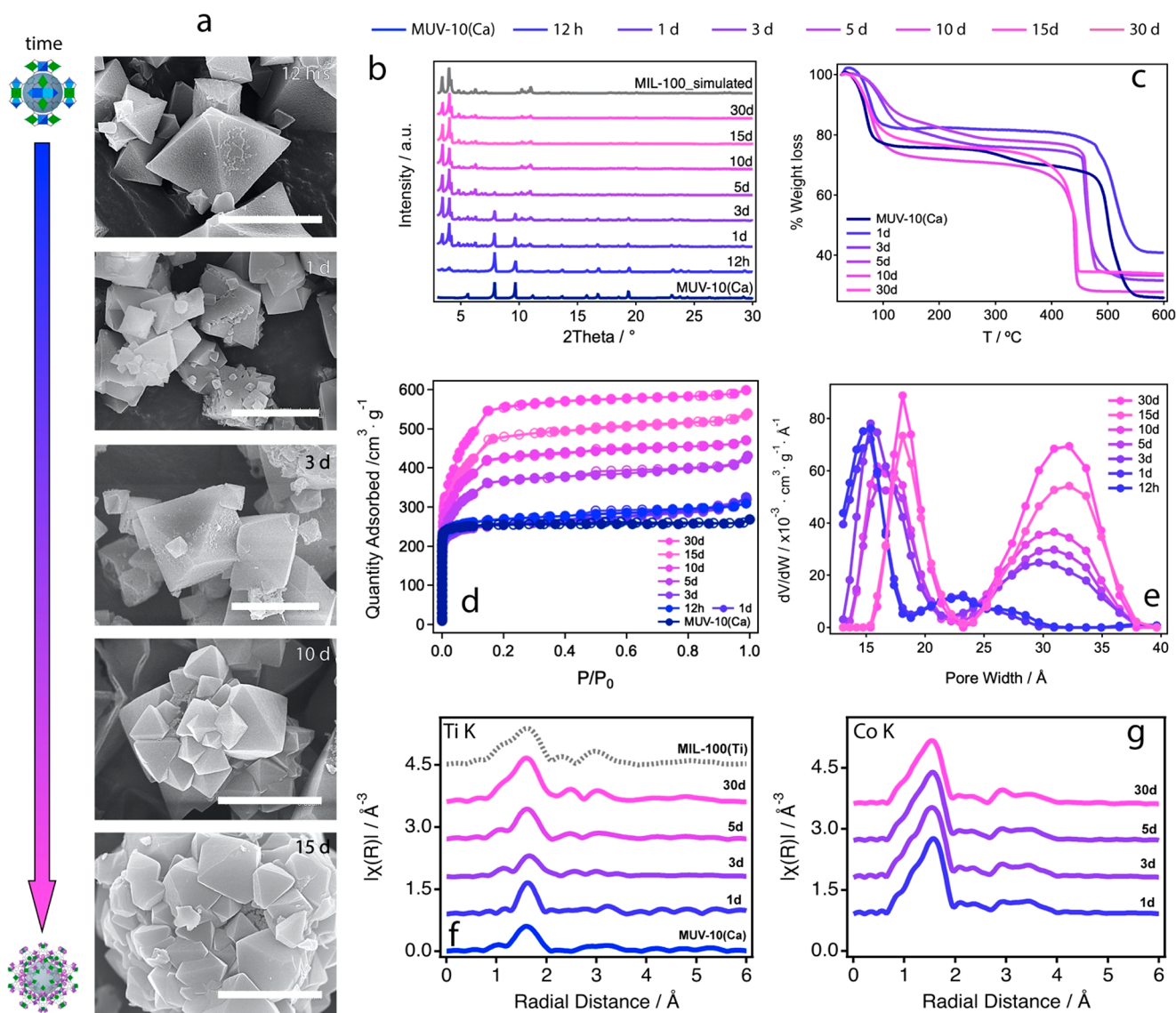
Figure 3. Dynamic topological transformation of MUV-10(Ca) to MUV-101(Co): (a) SEM images showing the progressive transformation of the crystals with time (scale bars 3 μm). Analysis of the transformation at different reaction times: (b) PXRDs showing the transformation of MUV-10(Ca) into MUV-101(Co) with time; (c) change in the chemical stability of the final material as result of the dilution of Ti−O bonds in TiCo$_2$ in comparison to Ti$_2$Ca$_2$ SBUs; (d) N$_2$ adsorption/desorption isotherms at 77 K showing the progressive increase in surface area with time; (e) pore size distribution (PSD) showing the evolution in pore size until the formation of a mesoporous framework; (f, g) EXAFS Ti and Co K-edge spectra of MUV-101(Co) at different stages of the transformation. The spectrum of MIL-100(Ti) was used for comparison and is shown as a dashed gray line. For a clearer analysis of the different stages of transformation see section S4 in the Supporting Information.

presence of Co^{2+}, MUV-10(Ca) seems to act as a templating scaffold that directs the growth of a new phase that we will refer to as MUV-101(Co). In fact, PXRD Rietveld refinement of this newly formed phase confirmed that transmetalation induces a topological change for the formation of a heterometallic titanium−organic framework isostructural with MIL-100 (zeotypic *mtn* topology; section S4.4 in the Supporting Information).[13]

Dynamic Topological Transformation of MUV-10 to MUV-101. We next investigated this phenomenon by isolating the crystals for different soaking times and analyzing the transformation at the different stages (section S4 in the Supporting Information). SEM images reveal the formation of a corrugated surface on the facets of MUV-10(Ca) crystals after 12 h of exposure to methanolic solutions of Co(II) (Figure 3a). We observe the formation of small crystallization

nuclei on the surface and edges of the crystal after 1 day, which evolve with time into micrometer-sized crystals with octahedral morphologies that can already be visualized after 3 days. Newly formed crystals seem to keep growing continuously at expense of the original MOF to produce a cluster of intertwined crystals after 15 days that keeps the original size and shape of the MUV-10(Ca) templating scaffold (Figure S55 in the Supporting Information). Overall, microscopic images suggest that both phases coexist and the formation of the MUV-101 phase proceeds by transformation of one crystal into the other rather than crystallization from redissolution of MUV-10 in the reaction medium. We cannot visualize the dissolution of the original crystals before the formation of the new crystals. Additional experiments with larger crystals show the particularities of the transformation more clearly (Figure S56 in the Supporting Information). This analysis was comple-

mented with EDX measurements as a function of the soaking time to account for the changes in chemical composition concomitant with the transformation of MUV-10 (section S4.2 in the Supporting Information). The data show a rapid incorporation of Co, which reaches a plateau at around 60 atom % after 15 days, parallel with the complete removal of calcium from the crystals. The relative titanium content decreases from 50 to 40 atom % until it stabilizes for a relative Ti:Co ratio close to 1:2. Single-point spectra of the chemical composition throughout the crystals are indicative of a homogeneous distribution of both metals in the expected ratio.

The study of the MUV-101 phase by single-crystal diffraction was not possible due to the intertwined nature of the crystals formed. Nevertheless, the structure was determined instead by refinement of high-resolution PXRD data collected by using synchrotron radiation (ALBA, BL04-MSPD) and using the structure reported for MIL-100(Ti) as a starting model (CCDC 1871195).[27] Rietveld refinement converged with excellent residual values (R_{wp} = 3.95%, R_{exp} = 1.77%) to a cubic $Fd\bar{3}m$ space group with the cell parameter a = 73.5784(8) Å (section S4.4 in the Supporting Information). MUV-101(Co) is isostructural with the prototypical MIL-100 family. Accordingly, heterometallic 6-c $TiCo_2$ SBUs are connected to six 3-c btc linkers to produce a zeolitic framework with an *mnt* topology, which combines two types of mesoporous cages of 2.4 and 2.9 nm interconnected in three dimensions. However, in MIL-100 phases, the introduction of M^{3+} (Cr, Fe, Al)[13,28,29] or M^{4+} (Ti)[27] metals into the homometallic SBU $[M_3(\mu_3\text{-}O)(X)(H_2O)_2(RCO_2)_6]$ is counterbalanced by the coordination of different capping linkers (X = F^-, Cl^-, OH^-, O^{2-}) to the axial position of the metal positions for a neutral structure. In MUV-101(Co), the combination of Co^{2+} and Ti^{4+} drives the formation of $[TiCo_2(\mu_3\text{-}O)(H_2O)_3(RCO_2)_6]$ clusters with possibly only water molecules acting as terminal ligands. The metallic ratio fixed by this formula agrees well with the experimental value determined by EDX. A phase transformation was also evaluated by PXRD of the crystals at increasing soaking times. Figure 3b shows that the [220] and [311] low-θ diffraction lines characteristic of the MUV-101 phase, isostructural with MIL-100, are already seen after only 12 h and become clearly visible after 1 day. From that point, MUV-10 and MUV-101 phases coexist up to 5 days of reaction, whereas the reflections [110] and [111] characteristic of MUV-10 are no longer visible. Rietveld refinements were used to calculate the relative phase percentages in these intermediate states. As shown in section S4.6 in the Supporting Information, the formation of MUV-101(Co) increases at the expense of MUV-10(Ca) for relative percentages of 3, 11, 65 and 98 atom % after 1, 3, 10, and 30 days, respectively.

The gradual conversion of the Ti_2Ca_2 cluster in MUV-10 into $TiCo_2$ in MUV-101(Co) is also correlated with changes in the thermal stability of the solid isolated at different reaction times. Thermogravimetric analyses (TGA; Figure 3c and section S4.7 in the Supporting Information) show a progressive decrease in the decomposition temperature upon incorporation of cobalt from 500 °C for MUV-10 down to a minimum of 440 °C in fully transformed MUV-101(Co) after 30 days. We argue that this is possibly due to the dilution of the relative percentage of robust Ti–O bonds in the metal–oxo clusters, which decreases from 45% in MUV-10(Ca) to 33% in MUV-101. Nonetheless, the thermal stability of MUV-101(Co) is significantly higher than that of other homometallic

phases such as as Fe^{3+} and Cr^{3+}, which decompose between 300 and 350 °C.[13,28] We next collected standard N_2 isotherms for all of the solids to investigate the effect of a phase transformation on their porosity (Figure 3d and section S4.8 in the Supporting Information). All solids display a type I isotherm with increasing gas uptakes for higher degrees of transformation. The reaction time gradually increases the multipoint BET surface area and pore volume values from 1054 $m^2 \cdot g^{-1}$ and 0.47 $cm^3 \cdot g^{-1}$ for MUV-101(Co)-12h, respectively, almost identical with those of the MUV-10(Ca) phase, to almost double these values for MUV-101(Co)-30d with 2043 $m^2 \cdot g^{-1}$ and 0.92 $cm^3 \cdot g^{-1}$. This value is consistent with the values reported for MIL-100 phases and confirms complete MOF-to-MOF conversion. The effect of this dynamic transformation on the porosity can be more easily visualized by looking into the pore size distribution (PSD). As shown in Figure 3e, at short reaction times between 12 h and 1 day the PSD is dominated by a broad distribution of micropores centered at 1.5 nm and incipient mesoporosity between 2 and 3 nm. This intermediate stage is reminiscent of MUV-10(Ca) with an incipient formation of MUV-101(Co) and agrees well with the coexistence of both phases anticipated by Rietveld analyses. The onset of mesoporosity is also consistent with the opening of a small hysteresis loop in the N_2 isotherm of these samples for the range P/P_0 = 0.4−1.0 (Figure S45 in the Supporting Information). From 3 days and onward the PSD reveals the formation of a mesoporous material with two pore sizes. The smaller pores increase up to 1.5−1.8 nm, whereas the largest pores lie close to 3.2 nm, consistent with the prevalence of the MUV-101 phase at these stages. Overall, the sorption data suggest that this topological transformation might be useful to gain dynamic control over the formation of hierarchical micro-/mesopore structures at intermediate stages of the transformation. We also confirmed that the stability of the final material toward water degradation was not compromised by running stability tests by soaking MUV-101(Co)-30d crystals in acid, neutral, and basic aqueous solutions (section S4.9 in the Supporting Information).

One of the main limitations in the synthesis of mixed-metal frameworks, by either direct or postsynthetic methods, is the likeliness of producing segregated single-component phases rather than a homogeneous distribution of the metals at an atomic level in the structure of the heterometallic MOF.[18] This problem is generally not discoverable by the characterization techniques used and requires more advanced tools such as X-ray absorption and high-resolution spectroscopies.[21] We used EXAFS (Ti and Co K-edges) to correlate the degree of transformation with the changes to the local composition and structure of the SBUs with time (Figure 3f,g and section S4.10 in the Supporting Information). Ti and Co K-edge EXAFS data collected on the MUV-101 phase at 77 K demonstrate the presence of heterobimetallic $TiCo_2$ clusters, with Ti–Co distances of ca. 2.94 Å (Table S8 in the Supporting Information). This intermetallic distance in the heterometallic cluster of MUV-101 is significantly shorter than the Ti–Ti distances seen in homometallic MIL-100(Ti) (i.e., 3.47 Å)[27] and agrees well with our DFT models and the crystallographic data reported for other heterometallic $TiCo_2$ clusters,[30] ruling out the formation of segregated phases. The detailed analyses of the Ti K-edge XANES region indicate the presence of a three-component pre-edge feature at 4971.5 eV after long transmetalation times, characteristic of centrosymmetric six-coordinated Ti^{4+} centers.[31,32] The intermediate stages of

transformation show more distorted octahedral geometries. With regard to the local structure of the cobalt centers in MUV-101(Co), Co K-edge XANES data show the presence of a pre-edge feature at 7709.2 eV after equivalent reaction times indicative of Co^{2+} with slightly distorted octahedral geometries, consistent with the formation of $TiCo_2$ clusters.[33] For a better understanding of the transformation process at the nanoscale, we next used scanning transmission electron microscopy (STEM) with EDX to collect high-resolution elemental maps throughout a slice of the crystals (Figure 4). MUV-101(Co)-
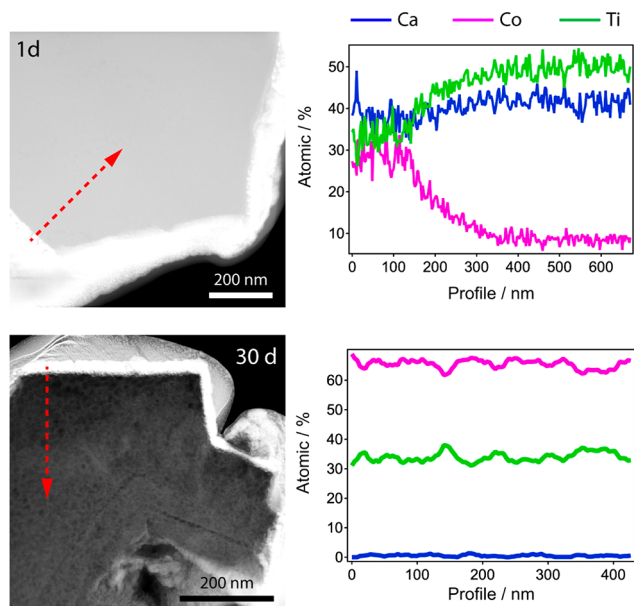

Figure 4. STEM-EDX of FIB-sectioned lamellae of MUV-101(Co)-1d and -30d showing the relative distribution of Ca (blue), Co (pink), and Ti (green) from the external surface to the inside of the crystal.

1d and -30d crystals were isolated, washed thoroughly, and sectioned with a focused ion beam (FIB). STEM-EDX of the lamellae at an early stage of the transformation confirms that the material grown on the external surface of the crystal is richer in cobalt and poorer in calcium in comparison to the interior. This spatial control over chemical composition agrees well with a diffusion-controlled process in which metal exchange induces the formation of MUV-101(Co) at the expense of MUV-10(Ca) crystals. We do not observe any signatures that account for the deposition of amorphous oxide coatings or segregation of phases, confirming the homogeneity of the process also at the nanoscale. Moreover, STEM-EDX spectral maps at different regions inside several crystals confirm the formation of a new material upon metal exchange with relative Ti, Co, and Ca contents consistent with the EDX analyses of bulk crystals (section S4.11 in the Supporting Information).

Origin of the Topological Transformation. To put our results in context, we looked at the literature for other examples of MOF transformations by metal exchange reactions. Zhang and co-workers recently reported the transformation of HKUST into MIL-100. In this case, the poor stability of HKUST in the reaction medium induces the decomposition and redissolution of the crystals by hydrolysis in the presence of Fe^{3+}, which is concomitant with the growth of nanoparticles of MIL-100(Fe).[34] In our case, the MOF transformation proceeds by crystal-to-crystal transformation

from a chemically stable precursor.[24] The epitaxial growth of MOFs first reported by Kitagawa and co-workers[35] involves exposure to metal solutions of MOF crystals with surfaces that are end-capped by linkers capable of coordinating the incoming metal. As a result, the outer surface of the crystal seeds the growth of an isostructural shell that is hybridized with the original core into a single mixed-metal crystal, provided there is an excellent match between both lattices. In our case, the crystals of MUV-10(Ca) (*the*; cubic, $Pm\bar{3}$, $a = 15.8362(8)$ Å) act as a templating scaffold and direct a topological transformation into MUV-101 (*mtn*; cubic, $Fd\bar{3}m$, $a = 73.5784(8)$ Å). In comparison to epitaxial growth, this process is driven by the generation of a new 6-c SBU, resulting in the formation of a new topology compatible with the structural information encoded in newly formed metal cluster and the 3-c organic linker common to both frameworks.

Intrigued by the differences with other MOF-to-MOF transformations available, we decided to rationalize the origin of this phenomenon by analyzing the surface terminations in MUV-10 crystals and studying the thermodynamics of the transformation of the SBU. We calculated the energies of (111), (001), and (110) surfaces representative of a cubic system with atomistic simulation techniques and used them to predict the equilibrium shape of the crystal through the Wulff construction method (see section S5 in the Supporting Information for computational methods).[36] As shown in Figure 5b, our results predict the formation of truncated octahedral crystals with preferential formation of (111) facets and small contributions from (001), with the latter being responsible for truncation of the octahedral symmetry. The expression of (001) facets is not visible from SEM pictures, which show MUV-10 crystals with regular octahedral morphologies (Figure 5a). This deviation from our model is possibly due to the effect of the solvent or the modulator (acetic acid) over the crystallization of the MOF, which was not considered in our calculations and might disfavor the stabilization of (001) surfaces. Accordingly, metal exchange reactions in MUV-10 shall be dominated by the terminations of the dominant (111) surfaces. Cleavage of the crystal along this direction by using the GDIS package[37] reveals the coexistence of exposed metal (ligand free) and ligand-capped terminations compatible with the ligand or metal-exchange reactions required for a structural transformation (Figure 5c,d). Similar terminations have been reported for other cubic MOFs such as UiO and HKUST.[38,39] To confirm this point, we performed additional metal exchange experiments with single crystals that reveal more clearly the nucleation of small seeds of MUV-101(Co) in the (111) facets of the octahedra (section S4.12 in the Supporting Information).

Our experimental results confirm the formation of heterometallic MUV-10(Mn) or MUV-101(Co) phases depending on the metal incorporated into the SBU. We hypothesized that an MOF-to-MOF transformation might be ascribed to the instability of the heterometallic Ti_2M_2 cluster that is generated when Ca^{2+} is replaced with Co^{2+} rather than Mn^{2+}. Accordingly, we calculated the energy balance for the replacement of Ca^{2+} nodes in $[Ti_2Ca_2(\mu_3\text{-}O)_2(H_2O)_4(RCO_2)_8]$ by these two metals. As shown in Figure 5e, the formation of an isostructural cluster is only thermodynamically favorable for Mn^{2+}, whereas it is disfavored for Co^{2+}. These differences likely originate from the higher preference of Ca and Mn for a 7-fold CTP coordination environment in comparison to other first-row transition-metal ions such as
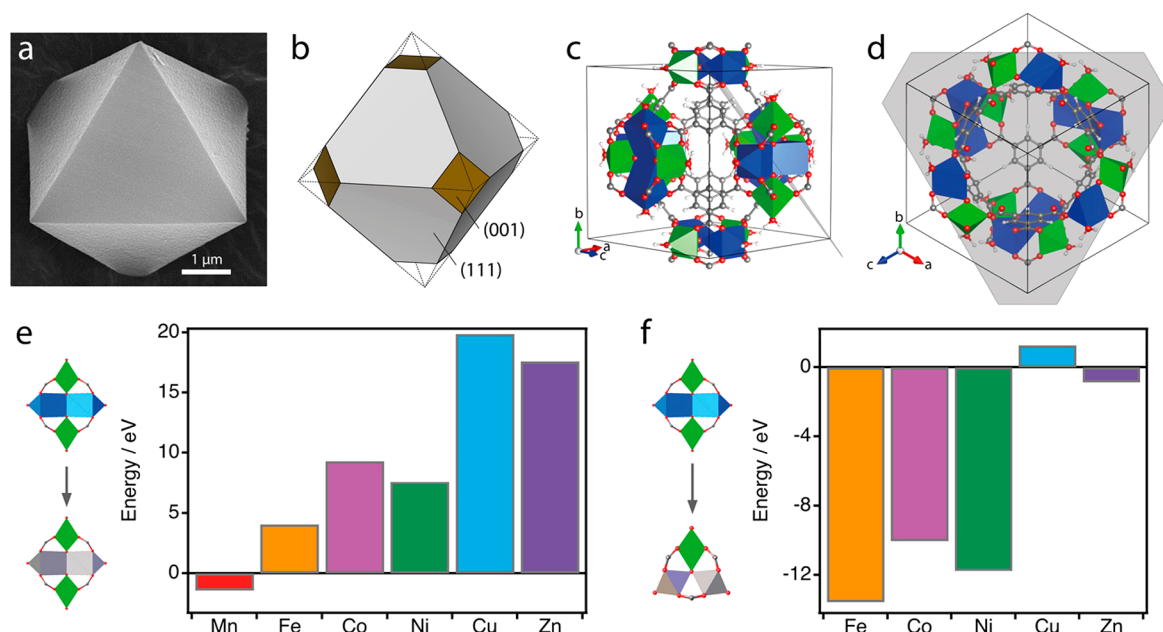
Figure 5. Origin of the topological transformation. (a) Experimental and (b) theoretical morphology of a crystal of MUV-10(Ca) calculated with the Wulff method. Differences are likely ascribed to the effect of the modulator used in the synthesis. (c) Perspective showing the cleavage of the cubic cell and the resulting (d) {111} surface termination combining metal and ligand free reactive sites. (e) Energy balance for the exchange of Ca^{2+} sites in $[Ti_2Ca_2(\mu_3\text{-}O)_2(H_2O)_4(RCO_2)_8]$ (Ti_2Ca_2) SBUs with Mn^{2+} (red), Fe^{2+} (orange), Co^{2+} (magenta), Ni^{2+} (green), Cu^{2+} (blue), and Zn^{2+} (purple). Except for Mn^{2+}, metal exchange would generate unstable coordination environments in isostructural clusters. (f) Enthalpy changes for the formation of $[TiM_2(\mu_3\text{-}O)(H_2O)_3(RCO_2)_6]$ (TiM_2) from Ti_2Ca_2 SBUs. Formation of TiM_2 metal−oxo clusters is disfavored for Cu^{2+} and thermodynamically possible for Fe^{2+}, Co^{2+}, Ni^{2+}, and Zn^{2+} with a significant preference for the first three.

cobalt. We ascribe these differences to changes in the ionic radii, which decrease from 1.06 and 0.90 Å for Ca^{2+} and Mn^{2+} to 0.65 Å for Co^{2+}.[40] In comparison to Co^{2+}, the electronic preference of Mn for this coordination geometry agrees well with the structural trends extracted from the Cambridge Structural Database for heptacoordination across the transition-metal series.[25] We argue that this thermodynamic instability triggers the transformation of Ti_2Co_2 into more stable $TiCo_2$ SBUs. This was further confirmed by calculating the enthalpy for the formation of $[TiCo_2(\mu_3\text{-}O)\text{-}(H_2O)_3(RCO_2)_6]$ from $[Ti_2Ca_2(\mu_3\text{-}O)_2(H_2O)_4(RCO_2)_8]$ clusters (Figure 5f), which indicates that the formation of the heterometallic $TiCo_2$ SBU is thermodynamically more favorable. Overall, this suggests that the transformation probably proceeds by metal exchange at the (111) surface of the crystal. Metal replacement would generate an offset in the coordination geometry of the Ti_2Co_2 heterometallic clusters that would evolve into the formation of more stable $TiCo_2$ SBUs. This would be the thermodynamic driving force guiding the formation of MUV-101(Co). In comparison to the microporosity of MUV-10(Ca), the mesoporosity of MUV-101(Co) shall enable more favorable diffusion of mass for quantitative transformation from the outside to the inside of MUV-10(Ca) crystals.

To gain a more general understanding of the effect of the metal over the transformation phenomenon, we extended the calculations to other common divalent first-row transition-metal ions (M^{2+} = Fe, Ni, Cu, Zn). Calcium exchange for the formation of heterometallic MUV-10(Ca) Ti_2M_2 clusters is also disfavored for these metals, following the order Cu > Zn ≫ Co > Ni > Fe with positive enthalpies of formation ranging from 19.9 to 4.1 eV for Cu and Fe, respectively (Figure 5e). These enthalpy changes are consistent with our previous

periodic calculations for metal exchange in MUV-10(Ca).[24,25] In turn, the calculated formation enthalpies of TiM_2 from Ti_2M_2 display different trends depending on the metal identity (Figure 5f). The formation of TiM_2 SBUs is thermodynamically more favorable for Fe, Ni, and Co, with energies ranging −13.6 to −10.0 eV, suggesting that these heterometallic phases of MUV-101 should also be synthetically accessible. However, the small stabilization for the formation of $TiZn_2$ (−0.9 eV) suggests that this material might be difficult to produce under thermodynamic control. Finally, Cu is the only metal for which the formation of the heterometallic trimer is not energetically favorable. This is in line with the low crystal field stabilization energies expected for Cu^{2+} and Zn^{2+}.[41] Given the instability of Ti_2Cu_2 SBUs, our simulations suggest that the exchange of MUV-10(Ca) crystals with copper might induce the formation of an alternative SBU for a different bipartite net compatible with the 3-c connectivity of btc linkers.

Effect of the Metal in Directing the Transformation. We performed additional metal exchange reactions to test the value of our theoretical predictions. MUV-10(Ca) crystals were soaked in concentrated solutions of Fe(II), Ni(II), and Zn(II) nitrate salts using the same conditions described above (section S6 in the Supporting Information). As anticipated by our calculations, all metals display a similar behavior and trigger the formation of colored crystals that are visible after 10 days, except for Zn. SEM-EDX and PXRD confirm the gradual exchange of Ca^{2+}, which becomes complete after 10 days for MUV-101(Zn) and 30 days for quantitative formation of crystals of MUV-101(Ni). MUV-101(Fe)-30d shows close to 13 atom % of calcium, indicative of an incomplete transformation, in good agreement with the presence of a residual fraction of the MUV-10 phase in the PXRD (Figure S61 in the Supporting Information). This is possibly due to the difficulties
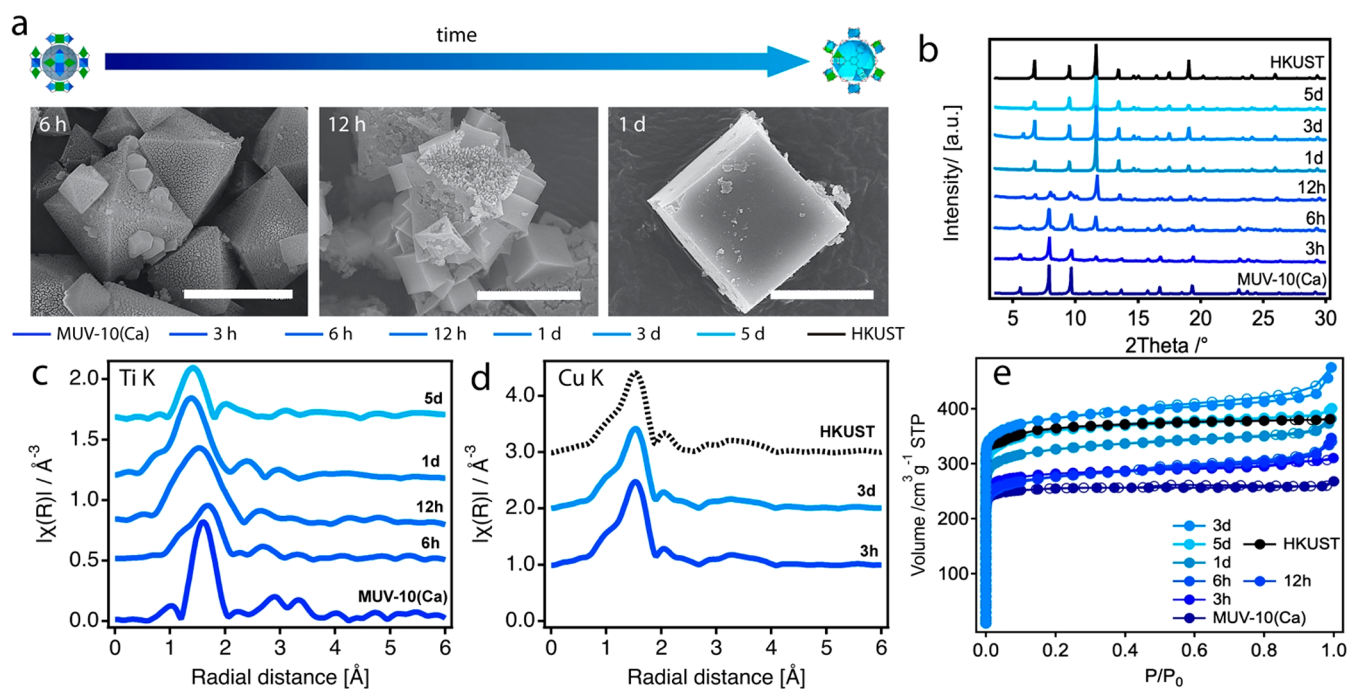
Figure 6. Dynamic topological transformation of MUV-10(Ca) to MUV-102(Cu). (a) SEM images showing the progress of the transformation with time for the formation of cubelike crystals of MUV-102(Cu) (scale bars 3 μm). Analysis of the MOF transformation at different reaction times: (b) PXRDs showing the transformation of MUV-10(Ca) into MUV-102(Cu) with time and comparison with commercial HKUST (black); (c, d) EXAFS Ti and Cu K-edge spectra of MUV-102(Cu) at different stages of transformation. The spectrum of homometallic HKUST was used for comparison and is shown as a dashed black line. (e) N$_2$ adsorption/desorption isotherms at 77 K showing the progressive increase in surface area and pore volume with time until they match those of HKUST (black line). For a clearer analysis of the different stages of transformation see section S7 in the Supporting Information.

in stabilizing Fe^{2+} in solution for the long reaction times used in the experiment. N$_2$ isotherms of MUV-101(Ni)-30d and MUV-101(Zn)-10d are indicative of mesoporous solids with BET values and pore sizes consistent with the formation of highly crystalline heterometallic MIL-100 phases. MUV-101(Fe)-30d shows a significantly smaller surface area as a result of the incomplete transformation. Overall, these results confirm the general value of MUV-10(Ca) as a precursor for inducing the formation of mesoporous, heterometallic titanium–organic frameworks by metal exchange at low temperature. To check if these phases were kinetic in nature, we also attempted to produce MUV-101(Fe,Co,Ni,Zn) MOFs by direct synthesis at high temperature. Whereas MUV-101(Fe,Co,Ni) can be prepared by solvothermal reactions of titanium isopropoxide with the metal salts and btc in DMF,[42] MUV-101(Zn) can only be isolated by a metal exchange reaction with MUV-10(Ca) at 65 °C. These results agree well with our theoretical predictions that reveal a clear thermodynamic preference for the formation of $[TiM_2(\mu_3-O)(H_2O)_3(RCO_2)_6]$ SBUs for Fe, Co, and Ni, whereas Zn is significantly less favorable.[25] As a result, this heterometallic phase can only be isolated by diffusion-controlled metal exchange rather than under thermodynamic control at high temperatures.

We next investigated the effect of Cu^{2+} on the transformation. Our calculations above suggest that the formation of TiCu$_2$ clusters is not favorable; therefore, we expected significant differences in the product of the metal exchange reaction. For a clearer overview of the process, we analyzed the progress of the reaction by isolating the product at different reaction times between 1 h and 5 days (section S7 in the Supporting Information). SEM measurements confirm the

formation of intertwined cubes at the facets of MUV-10(Ca) that become larger with time up to around 5 μm (Figure 6a). In comparison to MUV-101(Co), the reaction with Cu^{2+} is roughly 3 times faster. The copper content reaches a plateau close to 80% between 1 and 5 days, concomitant with the complete depletion of calcium from the crystals, for a final Ti:Cu ratio of close to 1:4 (section S7.2 in the Supporting Information). These differences in the morphology of the crystals and relative metal ratio in comparison to MUV-101(Fe,Co,Ni,Zn) indicated the formation of a different phase in the case of copper. This was first analyzed with PXRD (Figure 6b), suggesting complete transformation after 1 day into a highly crystalline material that we will refer to as MUV-102(Cu). Figure S81 in the Supporting Information shows the Le Bail refinement of the sample after 5 days, confirming that the resulting material is isostructural with HKUST (tbo; cubic, $Fm\bar{3}m$, a = 26.343(5) Å). This MOF is built from the linking of 4-c paddlewheel $[Cu_2(CO_2)_2(H_2O)_2]$ SBUs and 3-c btc organic molecules. The total metal content corresponds to the incorporation of 20 atom % of titanium in MUV-102(Cu), suggesting the formation of one heterometallic TiCu cluster per 2.5 homometallic Cu$_2$ units. Just as with MUV-101(Fe,Co,Ni,Zn) or MIL-100(Ti), we argue that the excess of positive charge that results from the replacement of Cu^{2+} with Ti^{4+} might be counterbalanced by the coordination of O^{2-} capping linkers to titanium for a heterometallic $[TiCu(RCO_2)_2(O)(H_2O)]$ SBU. The formation of a heterometallic cluster agrees well with the evolution of the Ti K-edge EXAFS data with the reaction time (Figure 6c,d), which indicate the presence of Ti–Cu distances at ca. 2.84 Å for long reaction times, in agreement with our DFT models for MUV-102(Cu) (Table S16 and section S7.6 in the Supporting Information).
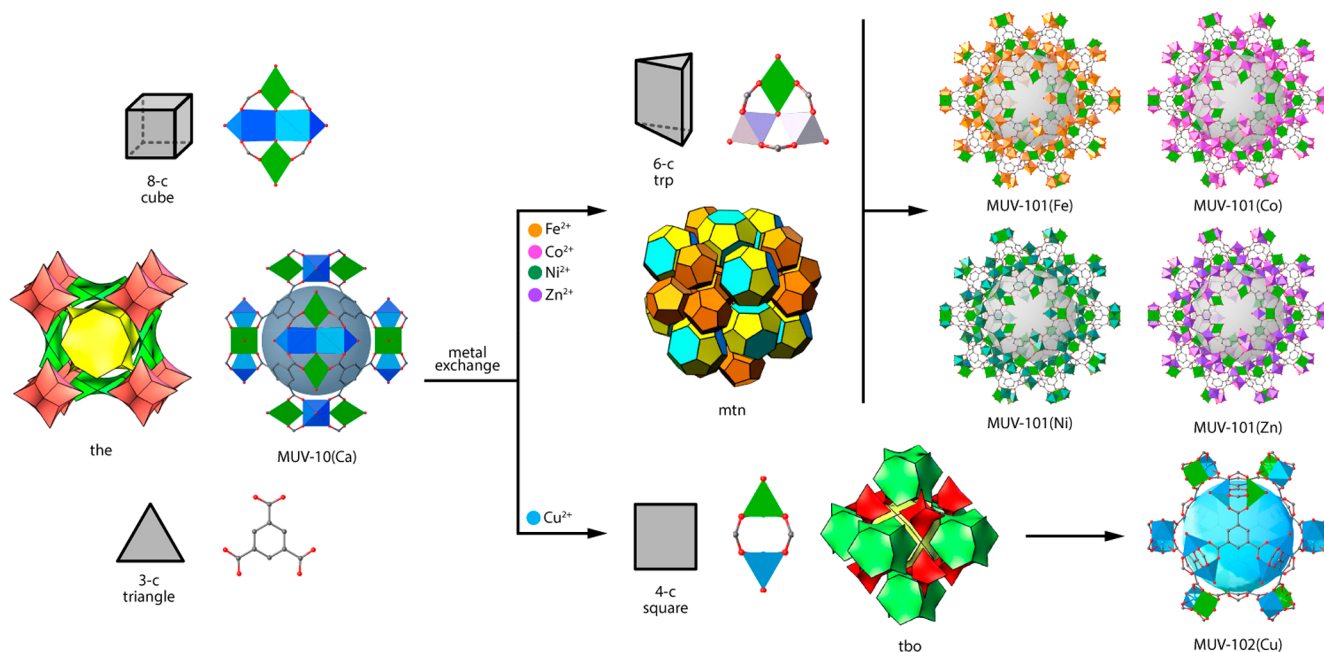
Figure 7. Topological transformation chart. Graphical overview of the binary heterometallic titanium—organic frameworks described in this work and their corresponding topologies and building units. By the principles of reticular chemistry, the transformation of the 8-c Ti_2Ca_2 metal—oxo cluster in MUV-10(Ca) into 6-c TiM_2 and 4-c TiCu units by metal exchange reactions drives the formation of the binary frameworks dictated by the local symmetries of 3-c btc units and the newly formed SBUs. All topologies shown have been taken from the Reticular Chemistry Structure Resource (RCSR; http://rcsr.anu.edu.au/).

Additionally, Ti and Cu K-edge XANES data demonstrated the simultaneous presence of highly distorted Ti(IV) six-[31,32] and five-coordinated Cu(II) centers[43,44] in MUV-102(Cu). The formation of heterometallic paddlewheel units is also consistent with the presence of uncoupled cupric $S = 1/2$ signals already present in the electron spin resonance spectra of MUV-102(Cu) after 6 h (section S7.7 in the Supporting Information). We discarded the formation of nanometer-thick oxide coatings upon transformation with STEM-EDX analyses. High-resolution spectral maps collected from FIB-sectioned crystals also confirm the formation of an outer shell of Cu that deepens into the crystal for increasing reaction times (section S7.8 in the Supporting Information). The formation of this binary *tbo* framework is consistent with N_2 gas sorption measurements. MUV-102(Cu) samples formed after transformations from 1 h to 5 days display type isotherms intrinsic to microporous materials with BET surface area values and pore sizes increasing from 1000 $m^2 \cdot g^{-1}$ and a micropore centered at 0.8 nm for MUV-102(Cu)-1h, characteristic of MUV-10, to 1509 $m^2 \cdot g^{-1}$ and bimodal microporosity centered at 0.9 and 1.1 nm after complete transformation in MUV-102(Cu)-5d. We measured the porosity of a commercial sample of HKUST (Basolite C300) soaked in MeOH for 5 days at room temperature to confirm the excellent match in porosity between both samples (Figure 6e and section S7.9 in the Supporting Information). The low titanium doping does not notably affect the thermal and chemical stability of MUV-102(Cu), which displays a decomposition temperature of 302 °C and the same limitations toward water hydrolysis as homometallic HKUST (sections S7.10 and S7.11 in the Supporting Information). As with MUV-101(Zn), we could not prepare this heterometallic analogue of HKUST by direct synthesis, confirming again the ability of metal-induced topological transformation to enable the formation of MOFs not accessible by *de novo* synthesis.

CONCLUSION

The synthesis of titanium frameworks still remains limited by the difficulties in controlling the high reactivity of Ti^{4+} ions in solution, which precludes the formation of persistent SBUs with the symmetry and connectivity required to target predefined topologies. We have shown the general value of MUV-10(Ca) as a precursor for directing the formation of mesoporous or microporous heterometallic titanium—organic frameworks at low temperature by exchange reactions with first-row transition metals. Metal exchange at the soft positions of the cluster induces a MOF-to-MOF transformation that is controlled by the formation of thermodynamically favored heterometallic clusters. As summarized in Figure 7, the nuclearity and nodes of connection of the resulting metal clusters are controlled by the metal incorporated and direct the assembly of binary frameworks according to the principles of reticular chemistry. In comparison to direct synthesis, this metal-induced topological transformation is a dynamic phenomenon and can be used to gain control over the formation of hierarchical micro-/mesopore structures by controlling the extent of transformation with time for the synthesis of mixed phases. Our results also suggest that this method enables the formation of heterometallic titanium MOFs that are not accessible under solvothermal conditions at high temperature, thus opening the door to the synthesis of additional titanium heterometallic phases not limited to trimesate linkers. On the basis of the advantageous properties of titanium and the intrinsic advantages of mixed-metal MOFs over their homometallic counterparts in applications such as gas storage/separation and heterogeneous catalysis,[18,19] we are confident that this approach might represent a turning point for the synthesis and general applications of titanium frameworks in a broad context.

■ ASSOCIATED CONTENT

Ⓢ Supporting Information

The Supporting Information is available free of charge at https://pubs.acs.org/doi/10.1021/jacs.0c00117.

Synthetic and experimental details, physical characterization, and supporting tables and figures as described in the text (PDF)

X-ray crystallographic data for MUV-101(Co) (CIF)

■ AUTHOR INFORMATION

Corresponding Authors

Natalia M. Padial − *Functional Inorganic Materials Team, Instituto de Ciencia Molecular (ICMol), Universitat de València, Paterna 46980, València, Spain;* ⓘ orcid.org/0000-0001-6067-3360; Email: nmpadial@scripps.edu

Carlos Martí-Gastaldo − *Functional Inorganic Materials Team, Instituto de Ciencia Molecular (ICMol), Universitat de València, Paterna 46980, València, Spain;* ⓘ orcid.org/0000-0003-3203-0047; Email: carlos.marti@uv.es

Authors

Belén Lerma-Berlanga − *Functional Inorganic Materials Team, Instituto de Ciencia Molecular (ICMol), Universitat de València, Paterna 46980, València, Spain*

Neyvis Almora-Barrios − *Functional Inorganic Materials Team, Instituto de Ciencia Molecular (ICMol), Universitat de València, Paterna 46980, València, Spain;* ⓘ orcid.org/0000-0001-5269-2705

Javier Castells-Gil − *Functional Inorganic Materials Team, Instituto de Ciencia Molecular (ICMol), Universitat de València, Paterna 46980, València, Spain;* ⓘ orcid.org/0000-0001-7931-3867

Iván da Silva − *ISIS Facility, Rutherford Appleton Laboratory, Didcot, Oxfordshire OX11 0QX, United Kingdom*

María de la Mata − *Departamento de Ciencia de los Materiales e I.M. y Q.I., Facultad de Ciencias, IMEYMAT, Universidad de Cádiz, 11510 Cádiz, Spain;* ⓘ orcid.org/0000-0002-1581-4838

Sergio I. Molina − *Departamento de Ciencia de los Materiales e I.M. y Q.I., Facultad de Ciencias, IMEYMAT, Universidad de Cádiz, 11510 Cádiz, Spain*

Jesús Hernández-Saz − *Departamento de Ingeniería y Ciencia de los Materiales y del Transporte, Escuela Politécnica Superior, Universidad de Sevilla, 41011 Sevilla, Spain;* ⓘ orcid.org/0000-0002-6630-7203

Ana E. Platero-Prats − *Departamento de Química Inorgánica and Condensed Matter Physics Center (IFIMAC), Universidad Autónoma de Madrid, 28049 Madrid, Spain;* ⓘ orcid.org/0000-0002-2248-2739

Sergio Tatay − *Functional Inorganic Materials Team, Instituto de Ciencia Molecular (ICMol), Universitat de València, Paterna 46980, València, Spain*

Complete contact information is available at:
https://pubs.acs.org/10.1021/jacs.0c00117

Author Contributions

●N.M.P. and B.L.-B. contributed equally.

Notes

The authors declare no competing financial interest.

■ REFERENCES

(1) Yaghi, O. M.; O'Keeffe, M.; Ockwig, N.; Chae, H.; Eddaoudi, M.; Kim, J. Reticular Synthesis and the Design of New Materials. *Nature* **2003**, *423*, 705−714.

(2) Mason, J. A.; Oktawiec, J.; Taylor, M. K.; Hudson, M. R.; Rodriguez, J.; Bachman, J. E.; Gonzalez, M. I.; Cervellino, A.; Guagliardi, A.; Brown, C. M.; Llewellyn, P. L.; Masciocchi, N.; Long, J. R. Methane Storage in Flexible Metal-Organic Frameworks with Intrinsic Thermal Management. *Nature* **2015**, *527*, 357−361.

(3) Tian, T.; Zeng, Z.; Vulpe, D.; Casco, M. E.; Divitini, G.; Midgley, P. A.; Silvestre-Albero, J.; Tan, J.-C.; Moghadam, P. Z.; Fairen-Jimenez, D. A Sol-Gel Monolithic Metal-Organic Framework with Enhanced Methane Uptake. *Nat. Mater.* **2018**, *17*, 174−179.

(4) Gu, C.; Hosono, N.; Zheng, J.-J.; Sato, Y.; Kusaka, S.; Sakaki, S.; Kitagawa, S. Design and Control of Gas Diffusion Process in a Nanoporous Soft Crystal. *Science* **2019**, *363*, 387−391.

(5) Li, L.; Lin, R.-B.; Krishna, R.; Li, H.; Xiang, S.; Wu, H.; Li, J.; Zhou, W.; Chen, B. Ethane/Ethylene Separation in a Metal-Organic Framework with Iron-Peroxo Sites. *Science* **2018**, *362*, 443−446.

(6) Cadiau, A.; Belmabkhout, Y.; Adil, K.; Bhatt, P. M.; Pillai, R. S.; Shkurenko, A.; Martineau-Corcos, C.; Maurin, G.; Eddaoudi, M. Hydrolytically Stable Fluorinated Metal-Organic Frameworks for Energy-Efficient Dehydration. *Science* **2017**, *356*, 731−735.

(7) Diercks, C. S.; Liu, Y.; Cordova, K. E.; Yaghi, O. M. The Role of Reticular Chemistry in the Design of CO2 Reduction Catalysts. *Nat. Mater.* **2018**, *17*, 301−307.

(8) Zhao, M.; Yuan, K.; Wang, Y.; Li, G.; Guo, J.; Gu, L.; Hu, W.; Zhao, H.; Tang, Z. Metal-Organic Frameworks as Selectivity Regulators for Hydrogenation Reactions. *Nature* **2016**, *539*, 76−80.

(9) Eddaoudi, M.; Kim, J.; Rosi, N.; Vodak, D.; Wachter, J.; O'Keeffe, M.; Yaghi, O. M. Systematic Design of Pore Size and Functionality in Isoreticular MOFs and Their Application in Methane Storage. *Science* **2002**, *295*, 469−472.

(10) O'Keeffe, M.; Yaghi, O. M. Deconstructing the Crystal Structures of Metal-Organic Frameworks and Related Materials into Their Underlying Nets. *Chem. Rev.* **2012**, *112*, 675−702.

(11) Kalmutzki, M. J.; Hanikel, N.; Yaghi, O. M. Secondary Building Units as the Turning Point in the Development of the Reticular Chemistry of MOFs. *Sci. Adv.* **2018**, *4*, No. eaat9180.

(12) Chui, S.; Lo, F.; Charmant, J.; Orpen, A. A Chemically Functionalizable Nanoporous Material [Cu$_3$(TMA)$_2$ (H$_2$O)$_3$]$_{(n)}$. *Science* **1999**, *283*, 1148−1150.

(13) Ferey, G.; Serre, C.; Mellot-Draznieks, C.; Millange, F.; Surblé, S.; Dutour, J.; Margiolaki, I. A Hybrid Solid with Giant Pores Prepared by a Combination of Targeted Chemistry, Simulation, and Powder Diffraction. *Angew. Chem., Int. Ed.* **2004**, *43*, 6296−6301.

(14) Férey, G.; Mellot-Draznieks, C.; Serre, C.; Millange, F.; Dutour, J.; Surblé, S.; Margiolaki, I. A Chromium Terephthalate-Based Solid with Unusually Large Pore Volumes and Surface Area. *Science* **2005**, *309*, 2040−2042.

(15) Cavka, J.; Jakobsen, S.; Olsbye, U.; Guillou, N.; Lamberti, C.; Bordiga, S.; Lillerud, K. A New Zirconium Inorganic Building Brick Forming Metal Organic Frameworks with Exceptional Stability. *J. Am. Chem. Soc.* **2008**, *130*, 13850−13851.

(16) Howarth, A. J.; Liu, Y.; Li, P.; Li, Z.; Wang, T. C.; Hupp, J. T.; Farha, O. K. Chemical, Thermal and Mechanical Stabilities of Metal-Organic Frameworks. *Nature Rev. Mater.* **2016**, *1*, 15018.

(17) Furukawa, H.; Cordova, K. E.; O'Keeffe, M.; Yaghi, O. M. The Chemistry and Applications of Metal-Organic Frameworks. *Science* **2013**, *341*, 1230444.

(18) Abednatanzi, S.; Derakhshandeh, P.; Depauw, H.; Coudert, F.-X.; Vrielinck, H.; Voort, P.; Leus, K. Mixed-Metal Metal-Organic Frameworks. *Chem. Soc. Rev.* **2019**, *48*, 2535−2565.

(19) Masoomi, M.; Morsali, A.; Dhakshinamoorthy, A.; García, H. Mixed-Metal MOFs: Unique Opportunities in Metal-organic Framework Functionality and Design. *Angew. Chem., Int. Ed.* **2019**, *58*, 15188−15205.

(20) Santaclara, J. G.; Olivos-Suarez, A. I.; Nelson, A.; Osadchii, D.; Nasalevich, M. A.; van der Veen, M. A.; Kapteijn, F.; eveleva, A.; Veber, S. L.; Fedin, M. V.; Murray, A. T.; Hendon, C. H.; Walsh, A.; Gascon, J. Revisiting the Incorporation of Ti(IV) in UiO-Type Metal-Organic Frameworks: Metal Exchange versus Grafting and Their Implications on Photocatalysis. *Chem. Mater.* **2017**, *29*, 8963−8967.

(21) Denny, M. S.; Parent, L. R.; Patterson, J. P.; Meena, S.; Pham, H.; Abellan, P.; Ramasse, Q. M.; Paesani, F.; Gianneschi, N. C.; Cohen, S. M. Transmission Electron Microscopy Reveals Deposition of Metal Oxide Coatings onto Metal-Organic Frameworks. *J. Am. Chem. Soc.* **2018**, *140*, 1348−1357.

(22) Das, S.; Kim, H.; Kim, K. Metathesis in Single Crystal: Complete and Reversible Exchange of Metal Ions Constituting the Frameworks of Metal-Organic Frameworks. *J. Am. Chem. Soc.* **2009**, *131*, 3814−3815.

(23) Brozek, C. K.; Dincă, M. Ti^{3+}, V$^{2+/3+}$, Cr$^{2+/3+}$, Mn^{2+}, and Fe^{2+} Substituted MOF-5 and Redox Reactivity in Cr- and Fe-MOF-5. *J. Am. Chem. Soc.* **2013**, *135*, 12886−12891.

(24) Castells-Gil, J.; Padial, N. M.; Almora-Barrios, N.; Albero, J.; Ruiz-Salvador, R. A.; González-Platas, J.; García, H.; Martí-Gastaldo, C. Chemical Engineering of Photoactivity in Heterometallic Titanium-Organic Frameworks by Metal Doping. *Angew. Chem., Int. Ed.* **2018**, *57*, 8453−8457.

(25) Cremades, E.; Echeverría, J. & Alvarez, S. The trigonal prism in coordination chemistry. *Chem. - Eur. J.* **2010**, *16*, 10380−10396.

(26) Brozek, C. K.; Dincă, M. Thermodynamic Parameters of Cation Exchange in MOF-5 and MFU-4 L. *Chem. Commun.* **2015**, *51*, 11780−11782.

(27) Castells-Gil, J.; Padial, N. M.; Almora-Barrios, N.; da Silva, I.; Mateo, D.; Albero, J.; García, H.; Martí-Gastaldo, C. De Novo Synthesis of Mesoporous Photoactive Titanium(IV)-Organic Frameworks with MIL-100 Topology. *Chem. Sci.* **2019**, *10*, 4313−4321.

(28) Horcajada, P.; Surblé, S.; Serre, C.; Hong, D.-Y.; Seo, Y.-K.; Chang, J.-S.; Grenèche, J.-M.; Margiolaki, I.; Ferey, G. Synthesis and Catalytic Properties of MIL-100(Fe), an Iron(Iii) Carboxylate with Large Pores. *Chem. Commun.* **2007**, 2820−2822.

(29) Volkringer, C.; Popov, D.; Loiseau, T.; Fěrey, G.; Burghammer, M.; Riekel, C.; Haouas, M.; Taulelle, F. Synthesis, Single-Crystal X-Ray Microdiffraction, and NMR Characterizations of the Giant Pore Metal-Organic Framework Aluminum Trimesate MIL-100. *Chem. Mater.* **2009**, *21*, 5695−5697.

(30) Hong, K.; Bak, W.; Moon, D.; Chun, H. Bistable and Porous Metal-Organic Frameworks with Charge-Neutral AcsNet Based on Heterometallic M$_3$O(CO$_2$)$_6$ Building Blocks. *Cryst. Growth Des.* **2013**, *13*, 4066−4070.

(31) Farges, F.; Brown, G. E. Coordination Chemistry of Titanium (IV) in Silicate Glasses and Melts: IV. XANES Studies of Synthetic and Natural Volcanic Glasses and Tektites at Ambient Temperature and Pressure. *Geochim. Cosmochim. Acta* **1997**, *61*, 1863−1870.

(32) Henderson, G. S.; de Groot, F.; Moulton, B. X-Ray Absorption Near-Edge Structure (XANES) Spectroscopy. *Rev. Mineral. Geochem.* **2014**, *78*, 75−138.

(33) Hunault, M.; Vercamer, V.; Haverkort, M.; Arrio, M.-A.; Brouder, C.; Calas, G.; Juhin, A. Tracking the Signature of Low Symmetry Environments in the XAS K Pre-Edge. *J. Phys.: Conf. Ser.* **2016**, *712*, 012005.

(34) Li, W.; Zhang, Y.; Zhang, C.; Meng, Q.; Xu, Z.; Su, P.; Li, Q.; Shen, C.; Fan, Z.; Qin, L.; Zhang, G. Transformation of Metal-Organic Frameworks for Molecular Sieving Membranes. *Nat. Commun.* **2016**, *7*, 11315.

(35) Furukawa, S.; Hirai, K.; Nakagawa, K.; Takashima, Y.; Matsuda, R.; Tsuruoka, T.; Kondo, M.; Haruki, R.; Tanaka, D.; Sakamoto, H.; Shimomura, S.; Sakata, O.; Kitagawa, S. Heterogeneously Hybridized Porous Coordination Polymer Crystals: Fabrication of Heterometallic Core-Shell Single Crystals with an In-Plane Rotational Epitaxial Relationship. *Angew. Chem., Int. Ed.* **2009**, *48*, 1766−1770.

(36) Herring, C. Some Theorems on the Free Energies of Crystal Surfaces. *Phys. Rev.* **1951**, *82*, 87−93.

(37) Fleming, S.; Rohl, A. GDIS: A Visualization Program for Molecular and Periodic Systems. *Z. Kristallogr. - Cryst. Mater.* **2005**, *220*, 580−584.

(38) Zhang, D.; Zhu, Y.; Liu, L.; Ying, X.; Hsiung, C.-E.; Sougrat, R.; Li, K.; Han, Y. Atomic-Resolution Transmission Electron Microscopy of Electron Beam-Sensitive Crystalline Materials. *Science* **2018**, *359*, 675−679.

(39) Amirjalayer, S.; Tafipolsky, M.; Schmid, R. Surface Termination of the Metal-Organic Framework HKUST-1: A Theoretical Investigation. *J. Phys. Chem. Lett.* **2014**, *5*, 3206−3210.

(40) Shannon, R. Revised Effective Ionic Radii and Systematic Studies of Interatomic Distances in Halides and Chalcogenides. *Acta Crystallogr., Sect. A: Cryst. Phys., Diffr., Theor. Gen. Crystallogr.* **1976**, *32*, 751−767.

(41) Cotton, A. F. I - Ligand Field Theory. *J. Chem. Educ.* **1964**, *41* (9), 466.

(42) Castells-Gil, J. M.; Padial, N.; Almora-Barrios, N.; Gil-San-Millán, R.; Torres, V.; Romero-Ángel, M.; da Silva, I.; Waerenborgh, J. C.; Jagiello, J.; Tatay, S. R.; Navarro, J. A.; Martí-Gastaldo, C. Heterometallic Titanium-Organic Frameworks as Dual Metal Catalysts for Synergistic Non-Buffered Hydrolysis of Nerve Agent Simulants. Submitted for publication (2020).

(43) Todaro, M.; Sciortino, L.; Gelardi, F.; Buscarino, G. Determination of Geometry Arrangement of Copper Ions in HKUST-1 by XAFS During a Prolonged Exposure to Air. *J. Phys. Chem. C* **2017**, *121*, 24853−24860.

(44) Borfecchia, E.; Maurelli, S.; Gianolio, D.; Groppo, E.; Chiesa, M.; Bonino, F.; Lamberti, C. Insights into Adsorption of NH$_3$ on HKUST-1 Metal-Organic Framework: A Multitechnique Approach. *J. Phys. Chem. C* **2012**, *116*, 19839−19850.